Miles, B. T., Hong, X., & Gersen, H. (2015). On the complex point spread function in interferometric cross-polarisation microscopy. Optics Express, 23(2), 1232-1239. 10.1364/OE.23.001232

On the complex point spread function in interferometric cross-polarisation microscopy

Benjamin T. Miles,[1] **Xin Hong,**[2,3] **and Henkjan Gersen**[1,*]

[1]*Nanophysics and Soft Matter Group, H.H. Wills Physics Laboratory, University of Bristol, Bristol, BS8 1TL, United Kingdom*
[2]*Department of Biomedical Engineering, Faculty of Electronic Informational & Electrical Engineering. Dalian University of Technology, Dalian, 116024, China*
[3]*hongxin@dlut.edu.cn*

**h.gersen@bristol.ac.uk*

Abstract: The ability to measure the Point Spread Function(PSF) is crucial in practical microscopy, but requires measuring the complex PSF for approaches that detect fields instead of intensities. Here we experimentally and theoretically model the volumetric amplitude and phase response of an Interferometric Cross-polarisation Microscope to demonstrate the technique's capability to provide confocal-like images of weakly birefringent structures in living cells. We find the axial FWHM of the amplitude PSF to be $0.70 \pm 0.01\,\mu m$ and $0.83\,\mu m$ for model and measurement, respectively, on par with confocal microscopy. Ultimately retaining both amplitude and phase information will however enable approaches for improved localisation of objects.

OCIS codes: ((180.1790) Confocal microscopy; (180.3170) Interferometric imaging; (260.5430) Polarization; (290.5850) Scattering, particles.

References and links

1. A. S. Stender, K. Marchuk, C. Liu, S. Sander, M. W. Meyer. E . A. Smith, B. Neupane, G. Wang, J. Li, J. Cheng, B. Huang, and N. Fang, "Single cell optical imaging and spectroscopy," Chem. Rev. **113**(4), 2469–2527 (2013).
2. G. Popescu, *Quantitative Phase Imaging of Cells and Tissues* (McGraw-Hill, 2011).
3. R. Oldenbourg, E. D. Salmon, and P. T. Tran, "Birefringence of single and bundled microtubules," Biophys. J. **74**(1), 645–654 (1998).
4. H. Inoue, T. Yoshioka, and Y. Hotta, "Membrane-associated Phospholipase C of Drosophila retina," J. Biol. **103**(1), 91–94 (1988).
5. R. Oldenbourg, "A new view on polarization microscopy," Nature **381**, 811–812 (1996).
6. J. R. Kuhn, Z. Wu, and M. Poenie, "Modulated polarization microscopy: a promising new approach to visualizing cytoskeletal dynamics in living cells," Biophys. J. **80**, 972–985 (2001).
7. P. C. D. Hobbs, "Heterodyne interferometry with a scanning optical microscope," Ph.D. Thesis, Stanford University (1987).
8. X. Hong, E. M. P. H. van Dijk, S. R. Hall, J. B. Götte, N. F. van Hulst, and H. Gersen, "Background-free detection of single 5 nm nanoparticles through interferometric cross-polarization microscopy," Nano Lett. **11**(2), 541–547 (2011).
9. B. T. Miles, E. C. Robinson, E. M. P. H. van Dijk, I. D. Lindsay, N. F. van Hulst and, and H. Gersen, "On the sensitivity of interferometric cross-polarisation microscopy," (to be submitted).
10. J. B. Pawley, *Handbook of Biological Confocal Microscopy*, third edition, (Springer, 2006).
11. C. M. Brown, R. W. Cole, and T. Jinadasa, "Measuring and interpreting point spread functions to determine confocal microscope resolution and ensure quality control," Nat. Protoc. **6**, 1929–1941 (2011).

12. P. Zijlstra and M. Orrit, "Single metal nanoparticles: optical detection, spectroscopy and applications," Rep. Prog. Phys. **74**(10), 106401 (2011).
13. K.Balman, and S. W. Hell, "Electric field depolarization in high aperture focusing with emphasis on annular apertures," J. Microsc. **200**(1), 59–67 (2000).
14. B. Richards and E. Wolf, "Electromagnetic diffraction in optical systems. II. Structure of the image field in an aplanatic system," Proc. R. Soc. A **253**(1274), 358–379 (1959).
15. M. R. Foreman, and P. Török, "Computational methods in vectorial imaging," J. Mod. Opt. **58**(5-6), 339–364 (2011).
16. L. Novotny and B. Hecht, *Principles of Nano-optics* (Cambridge University, 2012) Chap. 3.
17. S. W. Hell and E. H. K. Stelzer, "Properties of a 4Pi confocal fluorescence microscope," J. Opt. Soc. Am. A **9**(12), 2159–2166 (1992).
18. J. Hwang, and W.E. Moerner, "Interferometry of a single nanoparticle using the Guoy phase of a focused laser beam," Opt. Comm. **280**, 487–491 (2007).
19. M. Cagnet, M. Franon, J. C. Thrierr, *Atlas of Optical Phenomena* (Springer-Verlag, 1962)
20. A. Pralle, M. Prummer, E. -L. Florin, E. H. K. Stelzer, and J. K. H. Hörber, "Three-dimensional high-resolution particle tracking for optical tweezers by forward scattered light," Microsc. Res. Techniq. **44**, 378–386 (1999).
21. C. Macias-Romero, M. R. Foreman, R. T. Munro and P. Török, "Confocal polarization imaging in high-numerical-aperture space," Opt. Lett. **39**(8), 2322–2325 (2014).

The living cell is a fundamental yet complicated unit of interest to biology that is as important to a biologist as an atom is to a chemist [1]. To explain the inner workings of this basic unit, it is crucial to be able to visualize internal processes and structures with high contrast and resolution. The greatest obstacle to do this for living cells, without attaching contrast agents, is that generally cells do not absorb or scatter light significantly [2]. As a result one needs to rely on detecting changes in optical phase to generate contrast as is used in a variety of imaging techniques [1]. Polarized light microscopy forms a subset of these phase-sensitive techniques that has the potential to highlight specific structures, such as filaments and membranes, owing to their intrinsic optical properties [3, 4]. Although the potential for polarization microscopy to give valuable clues on the structure in living matter was realized decades ago, it still remains difficult to image weakly birefringent structures inside cells due to depolarization of light at lens surfaces and the weak signal levels when imaging through crossed polarisers [5, 6]. To address both these issues we recently introduced a novel confocal-like [7] microscopy approach, Interferometric Cross-Polarised Microscopy(ICPM) [8] that has already demonstrated the ability to resolve small polarisation signals against a large background using low incident power (1 μW) with an excellent extinction ratio [8, 9]. This will allow, for the first time, optical sectioning of weakly birefringent structures; however, to assess this capacity it is necessary to fully understand and characterise the technique.

It is well known that to correctly interpret images obtained in microscopy it is crucial to have a detailed understanding of the imaging and contrast mechanisms involved. Fortunately, in most practical applications, an imaging system such as a microscope can be approximated as a linear system. As a result, its imaging capabilities, such as resolution, are qualified by the Point Spread Function(PSF); the response of the microscope to an idealised point object. As the image of an arbitrary object is given by the convolution of the object with the PSF, the knowledge of the PSF in return allows the reconstruction of the object using deconvolution [10]. Hence the ability to measure the PSF in a practical microscope is of crucial importance [11]. However one should realize that in a microscope that relies on coherent detection of fields, such as ICPM, the system is linear in complex field not in intensities. Hence measuring the PSF in this type of microscopy requires the measurement of both the amplitude and phase of the PSF, which we in the following refer to as the complex PSF. Herein, we will show for the first time a direct measurement and modelling of the complex PSF for an Interferometric Cross-Polarised Microscope demonstrating that the obtained axial resolution is on par with classical confocal microscopy.

To measure the complex PSF of ICPM, we follow a similar approach to that recently detailed

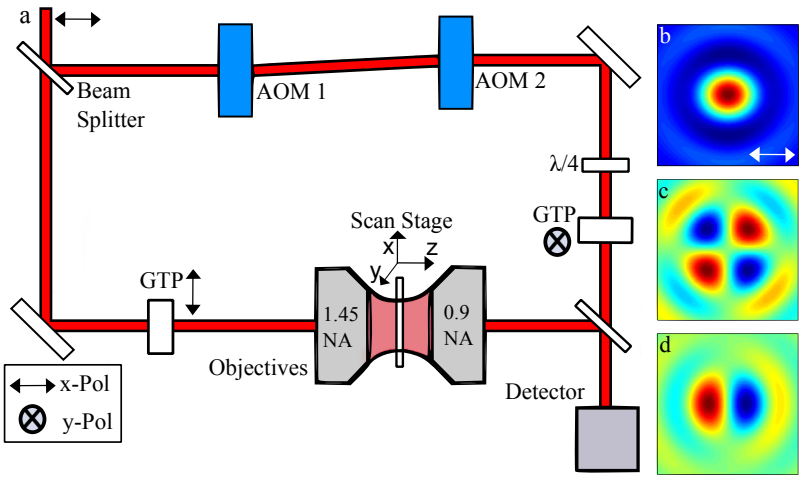

Fig. 1. (a) Schematic diagram illustrating Interferometric Cross-Polarised Microscopy. The light in the signal branch is focussed on the sample using a high NA objective and collected in transmission. The depolarisation effects of high numerical aperture focussing split incident polarised light into orthogonal components. (b) parallel, (c) perpendicular, and (d) axial polarisation components of the electric field relative to the incident polarisation are mapped for the NA=1.45 illumination objective (1 µm × 1 µm) at the focal plane [16]. By overlapping with a like-polarised reference, only the perpendicular polarisation component (c) is interferometrically enhanced leading to a background free detection scheme [8].

by Brown et al. [11] for measuring the intensity PSF. In order to probe both the amplitude and phase response of the complex PSF, we interferometrically detect the scattered signal from a sub diffraction-limit point source [12] as it is scanned through the focal volume. The selected point probe must be substantially smaller than the diffraction limit to resolve fine detail in the focal field. For this purpose, we elected to use commercially available monodisperse 10 nm diameter gold nanoparticles (BBI, U.K.). These particles were spin-coated on a size 1.5H (Marienfeld) glass coverslip that was surface-charged by a ten minute wash in a 1:2 part Sulfuric-Nitric acid bath before a 20 minute wash in deionised water. The producer quotes the acceptable mean particle size range as 9.0 nm to 11.0 nm with $< 10\,\%$ maximum acceptable $\%CV$. Similarly prepared samples were checked by AFM to ensure they were within the specifications and that they are deposited as isolated particles [8].

Our experimental approach is detailed in prior work [8], but was adapted for volumetric measurement by the addition of a 3D scanner, *PI P-733.3 XY(Z)*, for positioning the sample scanning stage, and an increased numerical aperture (NA = 1.45) for higher spatial resolution. Beyond this alteration the system remains, in working principle, the same and is schematically drawn in Fig. 1(a), with beam expanders omitted for simplicity. As shown, an *x*-polarised signal branch and *y*-polarised reference branch are frequency offset by a pair of acousto-optic modulators (AOMs) enabling heterodyne detection. Due to strong focusing by the illumination objective, the polarisation state of an incoming linearly-polarised beam is projected across all three axes, Fig. 1(b-d). In the presence of nanoparticles in the focus, these components are scattered to the far field; otherwise, the field is re-linearised by the collection objective [13]. As a consequence, orthogonal polarisations are only found in the far field when a nanoparticle is in the focal volume. Subsequently, the *y*-component of the focal field, Fig. 1(c), is selected by overlap with the like-polarised reference branch; providing interferometric enhancement only to photons that have impinged upon a nanoparticle [8]. The remainder of the sample illumina-

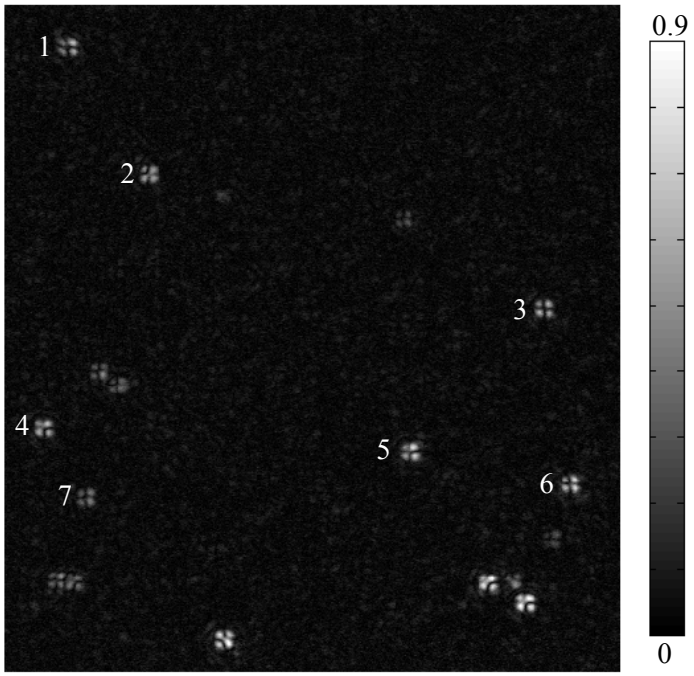

Fig. 2. ICPM detection of 10 nm diameter gold nanoparticles in the focal plane (*normalised*) showing light scattered by well isolated single particles (image-size: 18.51 µm × 20 µm, 512 × 512 pixels). The seven labelled particles, showing a typical single particle response, are used for a detailed comparison between measurement and model.

tion is orthogonal to the reference beam so does not contribute to the interferometric signal. In the idealised case of infinite extinction ratio polarisers, ICPM is therefore limited solely by the shot noise of the signal on the detector [9].

In order to measure the complex PSF, the sample was illuminated at 532 nm with a power prior to the illumination objective measured as 9 µW falling to 1.14 µW behind the collection objective. This power drop is a result of overfilling (filling factor = 1.7) of the illumination objective, internal reflections at the glass-air interface, and collection angles of the objectives. The reference branch power was 10 µW to ensure $E_{ref} >> E_{sig}$. The sample was scanned over an XY slice of 18.51 µm × 20 µm (fast axis and slow axis respectively) and digitally incremented along the optical axis (z) in 200 nm steps from 1 µm below to 1 µm above the focal plane. Scans were collected with 512×512 pixels at 0.4 s/line with a pixel dwell time of 0.7 ms and integration time of 366 µs. The midpoint of the z-axis scan range for the scanner controller was determined via observation of the back reflected light from the sample surface through the illumination objective. The collection objective was then focused on the sample, by checking for collimation of emerging light behind the collection lens.

An image was taken of the focal plane to observe the particle distribution; Fig. 2. The light scattered by individual nanoparticles in the image closely resembles the cloverleaf structure of the y-component of the focal distribution; showing that this field component is selected by the E_y polarised reference. Small asymmetries in scattered amplitude and structure are present in the sample set, which are attributed to the spread of particle sizes (10 ± 1 nm) and proximity to other particles as suggested in earlier work [8]. However, it is important to realise that the polarised detection scheme is sensitive to asymmetries in the shape of the particles which could

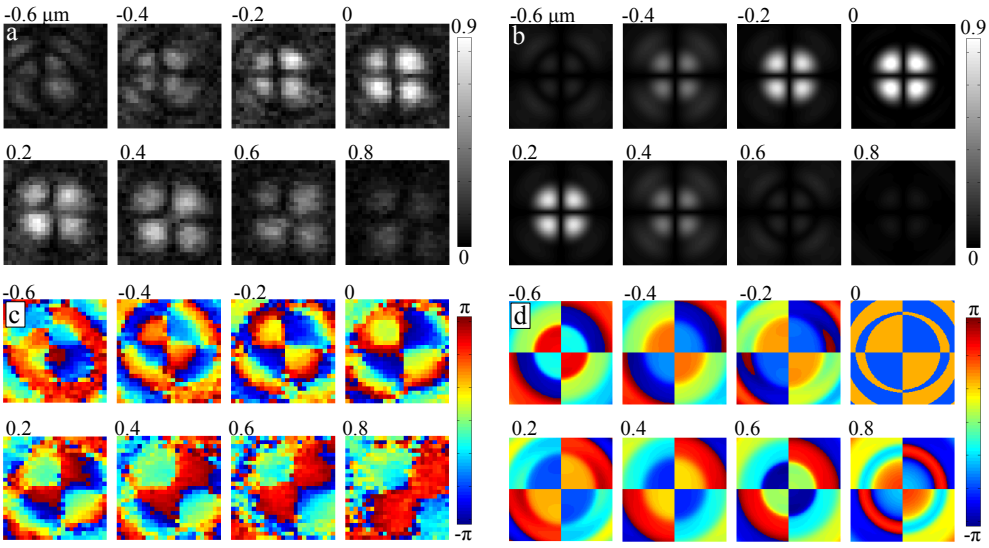

Fig. 3. Amplitude (*a, b*) and Phase (*c,d*) Response of Measurement (*left*) and Model (*right*). *Left*: A single particle's transit through the illumination volume (particle 3, Fig. 2) (0.97 µm × 1.0 µm). *Right*: Theoretical model generated for XY planes (1.0 µm × 1.0 µm) incremented along the optical axis (200 nm). Amplitudes have been normalised to the peak amplitude in the focus and labels indicate the distance from the focal plane in microns.

also contribute to the observed variations.

Results of measuring the complex PSF are displayed in the left panels of Fig. 3, and show the amplitude and phase for a stack of XY slices centred around a single particle as it is incremented along the optical axis. We display results on the same colour scale, where the label refers to the distance from the focal plane in microns with negative below and positive above the focal plane. The scan time for each plane is approximately four minutes and is performed twice at each axial position with time taken between scans to track laser power. The total time for the experiment was three and a half hours, so despite the system's stability some drift was unavoidable as evident from Fig. 3(a). The total displacement of the centre of the cloverleaf pattern is found to be 0.41 ± 0.04 µm in 3.5 h, which has not been corrected for in the images displayed. Note that this measurement time can be significantly reduced during routine operation to obtain a fast measurement for the complex PSF that is less affected by drift.

As a comparison for our experimental findings, the complex PSF of an idealised system was calculated using the theory of electromagnetic focusing of Richards and Wolf [14–16]. As we only interferometrically enhance a single field component, we consider that the complex PSF observed is returned through the interaction of the y-component of the illumination field and the y-polarised reference beam back-projected through the collection objective. This approach is specific to ICPM, but similar to that taken by Hell and Stelzer to determine the PSF of a 4Pi microscope [17], which also considers the general case of detecting randomly polarised emission photons. In cylindrical coordinates, the focal fields of an aplanatic lens, illuminated with x-polarised light with a given wavenumber, k, fill factor, f, object space refractive index, n_1, and image space refractive index, n_2, are given by;

$$E_{(\rho,\psi,z)} = \frac{ikf}{2} E_0 \sqrt{\frac{n_1}{n_2}} e^{-ikf} \begin{bmatrix} I_0 + I_2 cos2\psi \\ I_2 sin2\psi \\ -2iI_1 cos\psi \end{bmatrix}. \quad (1)$$

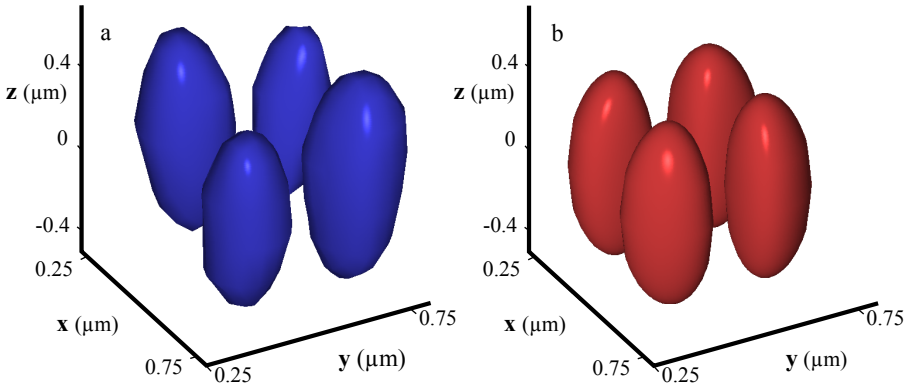

Fig. 4. A graphical illustration of the 3D amplitude PSF for (a) measurement and (b) model. The surfaces are constructed from a single particle's (particle 3, Fig. 2) transit through the focal volume using the slices presented in Fig. 3(a,b) respectively and surround a volume with greater than 40% of the peak amplitude. The amplitude PSF expresses as a cloverleaf structure extended along the z-axis with asymptotes of zero amplitude between the lobes.

Where the resultant integrals over incident illumination angle, θ, are;

$$\begin{aligned} I_0 &= \int_0^{\theta_{\max}} f_w(\theta)(cos\theta)^{\frac{1}{2}} sin\theta(1+cos\theta)J_0(k\rho sin\theta)\exp(ikzcos\theta)d\theta \\ I_1 &= \int_0^{\theta_{\max}} f_w(\theta)(cos\theta)^{\frac{1}{2}} sin^2\theta J_1(k\rho sin\theta)\exp(ikzcos\theta)d\theta \\ I_2 &= \int_0^{\theta_{\max}} f_w(\theta)(cos\theta)^{\frac{1}{2}} sin\theta(1-cos\theta)J_2(k\rho sin\theta)\exp(ikzcos\theta)d\theta \end{aligned} \quad , \tag{2}$$

with $NA = n\sin\theta_{max}$. Here, J_n are first order Bessel functions and $f_w(\theta)$ is the apodization function. These integrals are evaluated numerically over each field point in the XY plane at 200 nm increments along the optical axis from 1 μm below to 1 μm above the focal plane for both the illumination (NA=1.45) and collection (NA=0.9) objectives [16].

The complex PSF, $h_{xy}(z)$, can be reconstructed for each plane in the focal volume by multiplying the y-component of the illumination field, E_{ill}, with the y-component of the collection field, E_{det}, following the formalism:

$$h_{xy}(z) = E_{ill}(z) * E_{det}(-z), \tag{3}$$

where z selects the axial plane of interest between the two objectives focused at $z = 0$ [17]. From $h_{xy}(z)$ the interferometric amplitude and phase can be calculated. Fig. 3(b,d) shows the corresponding image stack of the interferometric amplitude and phase incremented through the focal volume over the same range as the presented measured data, showing excellent agreement between measurement and model. Note in particular the phase flip upon passing through the focal plane owing to the Guoy phase-shift [18] and the four fold symmetry associated with cross-polarised detection, Fig. 1(c). At the focal plane of Fig. 3(d), we probe the phase transition point of the Guoy phase-shift producing a sharp two-value image that in practice is difficult to obtain experimentally due to noise and experimental imperfections.

In order to further elucidate the agreement between measurement and model, a graphical representation of the 3D amplitude PSF is shown in Fig 4 for a single particle's transit through the focus (particle 3, Fig. 2) and the model. The volumes are constructed from the slices in Fig. 3(a)

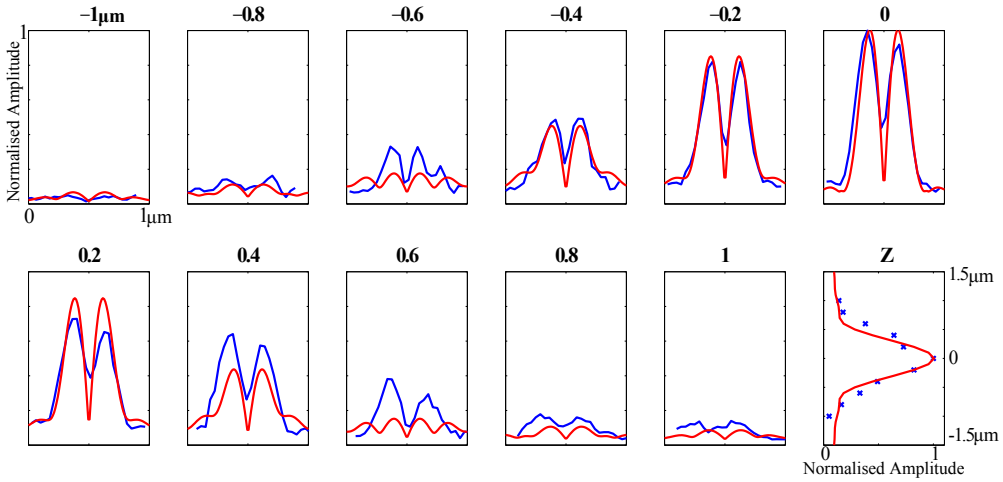

Fig. 5. Line scans averaged over the scattered amplitude signal from the seven labelled particles in Fig. 2 (*blue*) and corresponding model(*red*) for XY planes through the focal volume. The displayed amplitudes are normalised to the peak amplitude in the focal plane and labels indicate the distance to the focal plane in microns. The final panel (*Z*) shows the peak amplitudes of the preceding panels as a function of axial displacement. We find good agreement between data and model, which together demonstrate a sectioning capability on par with classical confocal microscopy.

and (b) for measurement and model respectively, after correcting for drift. The surfaces enclose a volume with greater than 40% the peak amplitude to extend the plots over a range of slices approximating the FWHM. Moreover, Fig. 5 presents line scans through the right hand lobes of the measured amplitude data averaged over seven particles (numbered in Fig. 2) compared to the model. At the focal plane, the FWHM of a single lobe of the scattered cloverleaf is found to be $2.13 \pm 0.05\,\mu$m compared to a theoretical expectation of $2.2 \pm 0.2\,\mu$m, which is in good agreement. The signal between the lobes of the clover leaf visible in Fig. 5(0 µm), is primarily the result of softening caused by averaging over the particle set, where the centre of each particle is only determined to a single pixel precision. In each axial slice, sharp phase transitions are present between lobes that point promisingly toward the prospect of improved transverse localisation [7]. Outside of the focal plane, when signal levels are low, there is some deviation between the data and model; particularly evident at $-0.6\,\mu$m and $0.6\,\mu$m where a larger amplitude is present in the measurement. This corresponds to broadening of the measured amplitude PSF, which we partially attribute to drift in the alignment between the objectives over the extended experimental time. However some asymmetry is also anticipated for both radial and axial measurements in the case of spherical aberrations that may result due to mismatch between refractive index and inconsistencies in immersion medium and coverslip thickness [19]. The absence of the phase switch in the measured data seen at $0.8\,\mu$m above the focal plane in the theoretical model compared to the measured data is also attributed to these two effects.

To extract the resolution of ICPM along the optical axis for the amplitude PSF, the FWHM is taken for the normalised amplitude data and theoretical model (including background) and found to be $0.83 \pm 0.02\,\mu$m and $0.70 \pm 0.01\,\mu$m respectively; Fig. 5(Z). The optical sectioning capacity is directly related to the FWHM of the amplitude PSF, so based on this measurement the system has an optical sectioning capability on par with classic confocal microscopy which reports an axial FWHM under similar conditions of approximately $0.7\,\mu$m. However it is im-

portant to realize that in contrast to a classical confocal, the measurement of both amplitude and phase enables approaches to improve both the axial and spatial resolution. One such approach relies on using the sharp phase-transition upon passing through the focal plane, which for example forms the basis of 3D particle tracking approaches [20]. Moreover, full knowledge of amplitude and phase allows for applying digital phase-filters to improve edge-responses as demonstrated experimentally by Philip C. D. Hobbs in reducing the axial resolution to $\lambda/4$ [7]. Combined these two approaches could provide significant improvements to the ability for particle localisation in contrast to classical intensity based measurements native to confocal microscopy [7].

Conclusion

To conclude, we have measured the full complex Point Spread Function of the Interferometric Cross-polarised Microscope and demonstrated excellent agreement with a model based on the theory of electromagnetic focussing. Both measurement and model reflect the strong axial confinement of the focal volume paving the way for future work applying this technique for confocal-like polarisation imaging of living cells. The complex PSF as measured and modelled in this paper is a crucial step to enable deconvolution of the obtained images to reconstruct objects of interest. Furthermore, recent work by Török et al. [21] showed that for polarised based detection schemes similar to the one shown here, the classical diffraction limit does not necessarily apply opening up intriguing avenues for future work.

Acknowledgments

This work was funded in part by the Biotechnology and Biological Sciences Research Council through a Technology Development Research Initiative (grant ref: BB/F004494/1) and carried out with the support of the Bristol Centre for Nanoscience and Quantum Information. X.H. acknowledges support by the National Natural Science Foundation of China (grant ref: 31271064).